J Mater Sci (2011) 46:7830–7838
DOI 10.1007/s10853-011-5764-5

Morphological comparison of isotactic polypropylene molded by water-assisted and conventional injection molding

Xianhu Liu · Guoqiang Zheng · Kun Dai · Zhenhua Jia · Songwei Li · Chuntai Liu · Jingbo Chen · Changyu Shen · Qian Li

Received: 2 June 2011 / Accepted: 30 June 2011 / Published online: 13 July 2011

Abstract It is well known that water-assisted injection molding (WAIM) process can be fulfilled based on the melt filling stage of conventional injection molding (CIM) process. However, due to the different physical fields involved during WAIM and CIM processes, WAIM part should exhibit unique morphological features compared with the CIM one. In this study, isotactic polypropylene (iPP) parts were prepared by WAIM and CIM, respectively, and their comparative study on morphology were therefore carried out by means of polarized optical microscopy (POM) and two-dimensional (2D) wide-angle X-ray diffraction (WAXD). POM observations illustrated that the WAIM part exhibits a "skin–core–water channel" structure, while the CIM part shows a typical "skin–core" structure. 2D-WAXD results showed obvious arclike reflections in each position along thickness direction of the WAIM part, indicating a pronounced molecular orientation. Furthermore, a parent–daughter model (or branched shish-kebab structure) appears at 0 and 100 μm for both the parts, and the fraction of daughter lamellae for WAIM part is lower than that of CIM part. As for the 1D-WAXD curves, it is noticed that there is a very tiny (300) reflection of β-form in the CIM part, while it is invisible in all positions of the WAIM part. In addition, the crystallinity and crystalline size L of CIM part are found to be higher than that of WAIM part. Those results demonstrate that water penetration and rapid cooling rate have a significant effect on the morphological features of WAIM part.

Electronic supplementary material The online version of this article (doi:10.1007/s10853-011-5764-5) contains supplementary material, which is available to authorized users.

X. Liu · G. Zheng (✉) · K. Dai · Z. Jia · S. Li · C. Liu (✉) · J. Chen · C. Shen · Q. Li
College of Materials Science and Engineering,
The Key Laboratory of Advanced Materials Processing & Mold of Ministry of Education,
Zhengzhou University, Zhengzhou 450002,
People's Republic of China
e-mail: gqzheng@zzu.edu.cn

C. Liu
e-mail: ctliu@zzu.edu.cn

Introduction

Water-assisted injection molding (WAIM), an innovative injection molding technique [1–6], has gradually become one of the most important methods producing hollowed plastic parts. One of the typical WAIM processes, illustrated in Fig. 1a, can be described as follows. Firstly, the cavity is partially filled (short-shot) with polymer melt. Secondly, the pressurized water is injected into the core of the polymer melt and assists the melt to fill the cavity. Finally, the injected water continues to pack the melt till the melt is fully solidified. Recently, because of the light weight of WAIM products, relatively lower resin cost per part, shorter cycle time, as well as its flexibility in the design and manufacture of plastic parts [1–9], WAIM has received great interests.

So far, the crystalline morphology of the semi-crystalline polymers molded by conventional injection molding (CIM) has been studied intensively. Numerous researchers have demonstrated that the shear stress in CIM process has significant effect on the subsequent development of crystalline structure and orientation [10–17]. For example, in the case of isotactic polypropylene (iPP) molded by CIM, quite apparent orientation is fabricated in the skin layer, and furthermore, some shish or shish-kebab structure is always observed due to the combined effect of strong shear flow and fast cooling rate at the melt filling stage [12, 16].

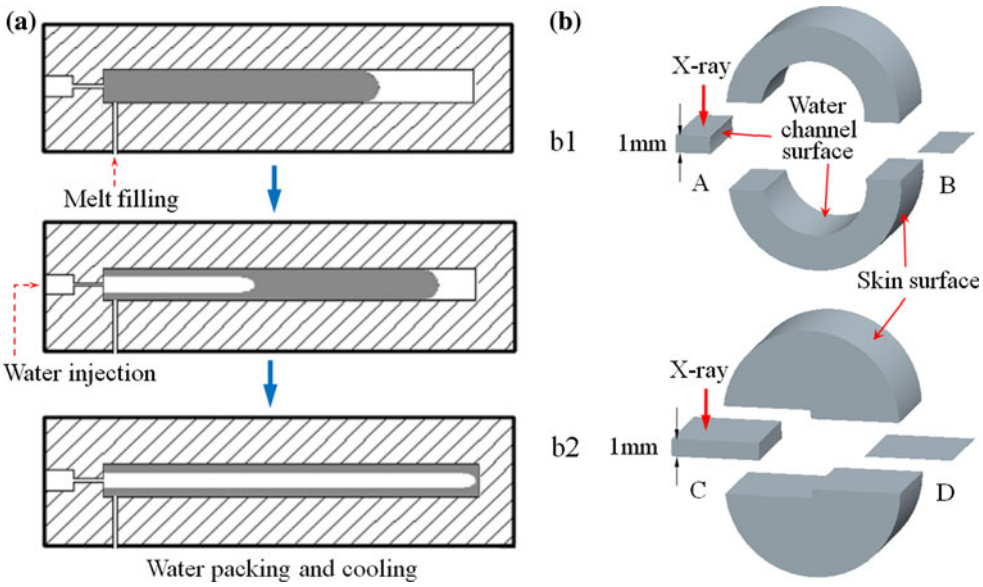

Fig. 1 Schematic of WAIM process based on short-shot (**a**) and the samples preparation of WAIM part (**b**1) and CIM part (**b**2) for 2D-WAXD measurements (*A*, *C*) and POM observation (*B*, *D*)

However, because of shear flow attenuation and temperature gradient from skin to core, spherulites or randomly distributed lamellae are formed in the core region. Over the years, the hierarchical structure and crystalline morphology of injection molded parts have been intensively characterized. The dispersed phase morphology of polymer blends in WAIM parts has been studied by Liu et al. [5, 6] and Huang and Zhou [7]. However, to the best of our knowledge, crystalline morphology developed during the complex processing conditions in WAIM process is scarcely reported in the open literatures.

In our previous study [9], the hierarchical structure and crystalline morphology of high density polyethylene (HDPE) molded by WAIM was studied solely by 2D-SAXS. The results showed that the shish-kebab structure is formed in the skin and water channel zones because of the shear stress brought by the melt filling and water penetration, respectively. Obviously, it is limited to present the panorama of the morphological features and their distribution of other semi-crystalline polymers molded by WAIM.

It is well known that iPP has good comprehensive properties, thus iPP is widely used as a commodity plastic. Moreover, iPP is a polymorphic material with several crystal modifications, including monoclinic α-phase, the trigonal β-phase, the orthorhombic γ-phase, and smectic mesophase. Thus, iPP is always used as representative template to study the crystalline evolution during CIM process. Considering that WAIM process can be fulfilled based on the melt filling stage for CIM process, in the present study, the crystalline morphology of pure iPP molded by WAIM is therefore investigated through comparison with that of the corresponding CIM part.

Experimental part

Material

Commercially available iPP (T30S) was purchased from Lanzhou Petroleum Chemical Co., China. Its $\overline{M}_n$ and melt flow index is ca. 11.0×10^4 g/mol and 2.6 g/10 min (190 °C, 21.6 N), respectively.

Sample preparation

A home-made water injection unit, consisting of a pressurized water generator, a conveying unit, and an injection pin, was developed based on a pressurized water system (Maha, M16/9, Italy) in our laboratory. The water injection pin is of orifice type, whose inner diameter is ca. 0.5 mm. A HTF80B-W2 injection molding machine (Haitian, China) was used for melt injection. In order to provide a route for water penetration, the main bodies of both WAIM and CIM parts were designed into a cylindrical shape, with a diameter of 10 mm and a length of 300 mm. The difference between them is that the CIM part exhibits a solid structure, while the WAIM part has a hollowed one. The thickness of the residual wall for WAIM part is about 1.6 mm.

The barrel temperature of the injection molding machine was 170, 185, 205, and 200 °C, respectively, from the hopper to nozzle. Both mold and injected water were kept at room temperature. The melt injection and the water injection pressures were 60 and 15 MPa. Other processing parameters, e.g., the water injection delay time is 2 s, and short-shot size is 80 vol%. The processing parameters used for CIM parts were generally the same as the WAIM part,

except that no water injection and packing was applied on the former.

Characterization

The Macroscopic hierarchical structure of iPP molded by WAIM and CIM were investigated via polarized optical microscope (OLYMPUS BX61). The sample slice with a thickness of 10 μm was cut from the middle of the part (see Fig. 1b), and placed between the two glass slices.

2D-WAXD measurements were employed to characterize the crystalline structure and molecular orientation distribution of WAIM part. 2D-WAXD patterns were collected in a scattering beamline at the National Synchrotron Radiation Laboratory, University of Science and Technology of China, Hefei. The chosen X-ray wavelength λ was 1.54 Å, where the sample to detector distance was 400 mm. A MAR 345 image plate detector was employed to collect all the 2D-WAXD images. The sample preparation and the selected region for 2D-WAXD measurements are illustrated in Fig. 1b.

Results and discussion

Macroscopic hierarchical structure

The macroscopic hierarchical structure of iPP molded by WAIM in thickness direction is shown in Fig. 2. The thin, oriented skin layer and water channel zone, as well as an anisotropic intermediate zone can be observed. In the magnified micrographs of the region near the skin surface (left bottom) and water channel surface (right bottom), it is found the thickness of the oriented skin zone and water channel zone is about 50 and 20 μm, respectively. Some small spherulites of varying sizes can be observed in these regions. Unfortunately, the size of these spherulites is too small to be determined. Nonetheless, the spherulites near the water channel zone are slightly larger than those in the skin zone, showing a different micromorphology. As shown by the higher magnified intermediate zone (middle bottom), comparatively large spherulites can be observed, and the diameters of the spherulites are around 10–40 μm.

As clearly shown in Fig. 1a, after the melt filling, pressurized water penetrates subsequently in the core of melt. It is certain that the rapid cooling rate brought by the injected water will dramatically affect on the interior melt. The melt in skin and water channel regions has a higher cooling rate, which induces a higher nucleation density [10]. Thus, a large number of very small spherulites develop in the skin and water channel zones, and fewer but larger spherulites appear in the intermediate zone.

As mentioned above, the thermo-mechanical field in WAIM process is more complicated than that in CIM process. It can be envisaged that a more distinct morphology will be developed during WAIM process due to the water penetration. It is therefore interesting to make a comparison between WAIM and CIM parts for the better understanding of the crystalline morphology evolved during WAIM process. Figure 3 shows the typical skin–core hierarchical structure of the CIM part, which is characterized clearly by two distinct regions: an oriented skin zone and a spherulitic core with essentially no preferred orientation (referred as ‘‘core zone’’). Apparently, the size of spherulites increases gradually from the skin to core zone.

Similarly, in the skin zone for both the parts, the tiny crystallites are formed, but the crystallites in the CIM part are somewhat larger than those in the WAIM part. Besides,

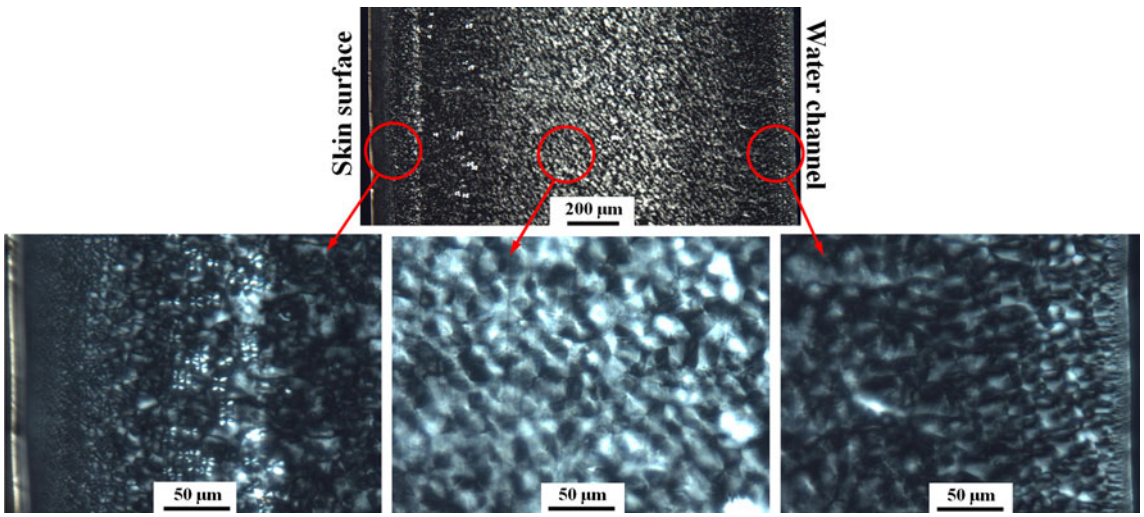

Fig. 2 POM micrographs of skin–core-water channel crystalline structure of WAIM part. The flow direction is vertical

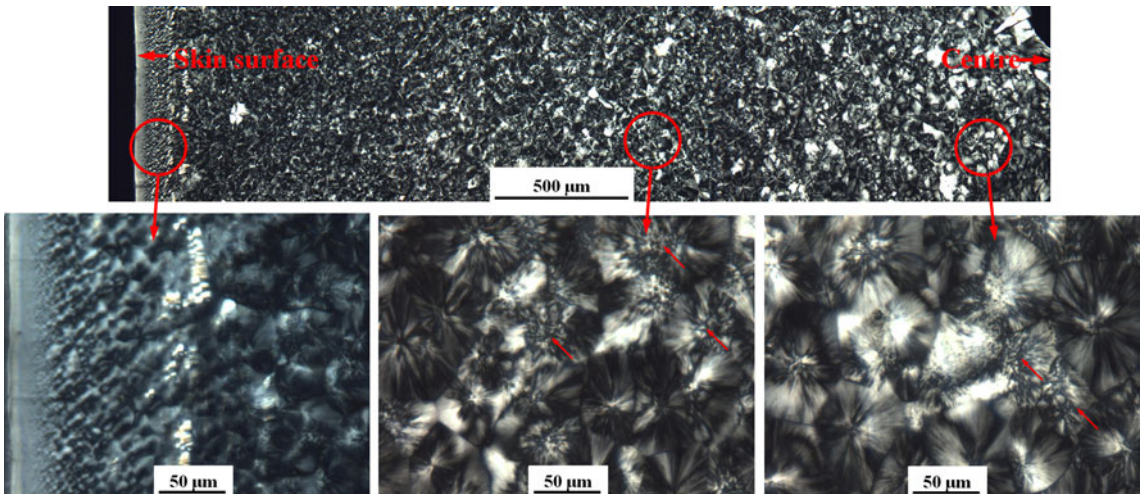

Fig. 3 POM micrographs of skin–core crystalline structure of CIM part. The flow direction is vertical

the skin zone has basically no obvious change in thickness compared with that of WAIM part. In the core zone, the average diameter of CIM spherulites is much larger than that of WAIM spherulites in the intermediate zone. The lower level of shear and smaller cooling rate in the core zone of CIM part, allowing a longer time to grow into big spherulites, is responsible for this phenomenon. Interestingly, β-form-like crystals with loosely packed lamellae is easily distinguished in CIM part (shown by the arrows in Fig. 3), especially in the region away from skin surface. However, they are scarcely seen in WAIM part.

Orientation

In order to better understand the orientated crystallization, WAIM and CIM parts were characterized by 2D-WAXD measurements. For a brevity purpose, the WAXD measurements were taken at 0, 100, 800, 1500, 1600 μm (i.e., water channel surface) for the WAIM part, and 0, 100, 800, 1600, 5000 μm (i.e., the core) for the CIM part, respectively, in the thickness direction. The "0 μm" is defined as the first signal picture by 2D-WAXD measurements from the outer surface (i.e., skin surface) for both the parts.

Figure 4 shows the WAXD patterns at the selected positions of WAIM and CIM parts. For both the parts, the diffraction intensity distribution consists of five diffraction rings associated with different lattice planes of iPP, corresponding to (110), (040), (130), (111), and (131) from inner to outer circles, respectively, which are the characteristic of α-phase crystals. At a given position, the reflections of WAIM part show a much stronger azimuthal dependence than those of the CIM part, indicating a higher level of molecular orientation. Whereas for CIM part (see Fig. 4b), the arclike reflection is only seen at 0 and 100 μm, and the isotropic rings can be visibly seen in other positions due to chain's random orientation. Especially, the parent–daughter model (or branched shish-kebab structure), determined by the (110) reflection, appears at 0 and 100 μm for both the parts.

In order to quantitatively estimate the molecular orientation in different positions of the WAIM and CIM parts, the azimuthal patterns of the (040) reflection at different distances are illustrated in Fig. 5. The molecular orientation is estimated using the Hermans orientation function by [18],

$$f = \frac{3\langle \cos^2 \varphi \rangle - 1}{2} \tag{1}$$

$$\langle \cos^2 \varphi \rangle = \frac{\int_0^{\pi/2} I(\varphi) \cos^2 \varphi \sin \varphi \mathrm{d}\varphi}{\int_0^{\pi/2} I(\varphi) \sin \varphi \mathrm{d}\varphi} \tag{2}$$

where φ is the angle between the normal of a given ($hk0$) crystal plane and the flow direction, and I is the intensity. The critical values of orientation function f, taking $\varphi = 0$ as the flow direction, are -0.5 for a perfect perpendicular orientation and 1.0 for a perfect parallel orientation. The orientation parameter for the (040) plane of α-crystal was calculated according to Eqs. 1 and 2, and the values are listed in Table 1. Obviously, except for the position at 0 and 100 μm, the orientation parameter for the WAIM part is considerably larger than that of the CIM part. It is generally accepted that the molecular orientation in the skin zone is mainly attributed to the melt filling, and thus, it is understandable that there should be no notable difference in orientation in the region. However, due to the high cooling rate brought by injected water for WAIM part, the slightly large molecular orientation in the skin zone can be formed. More interestingly, in the case of the WAIM part, the orientation parameter is remarkably enhanced at 1500 and 1600 μm because of the shear stress and rapid cooling

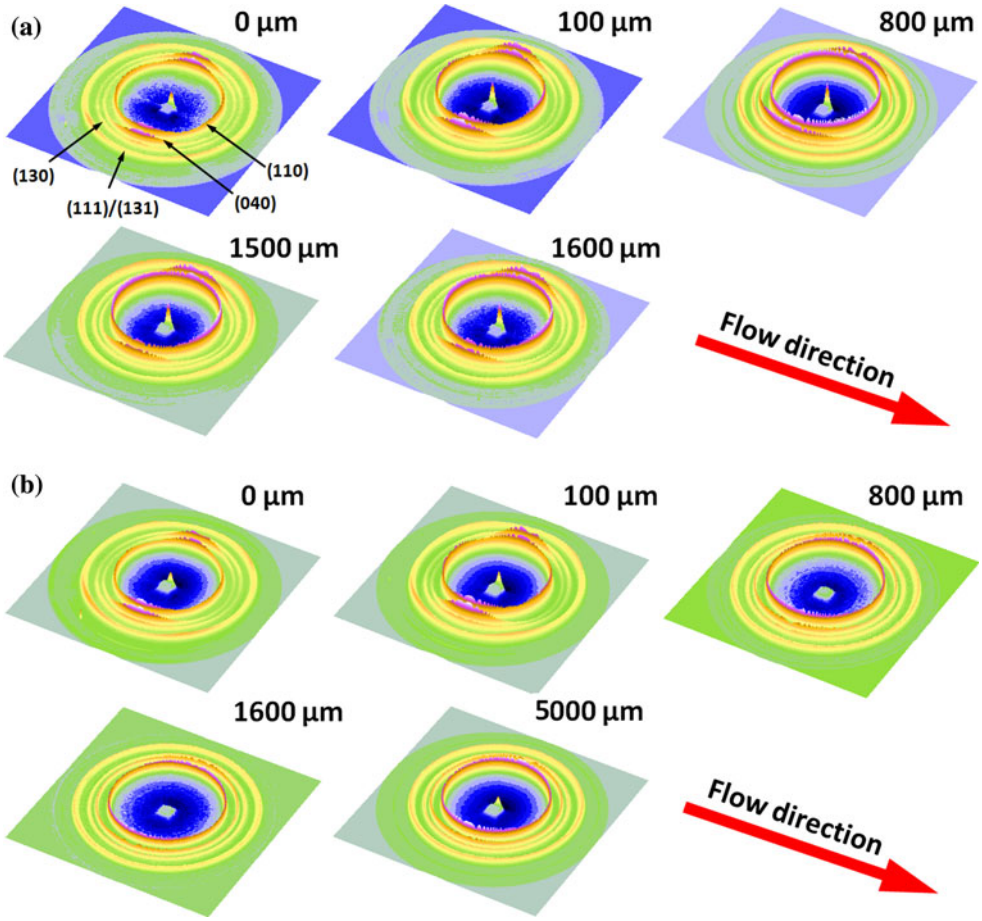

Fig. 4 2D-WAXD patterns at selected positions of (**a**) WAIM part and (**b**) CIM part

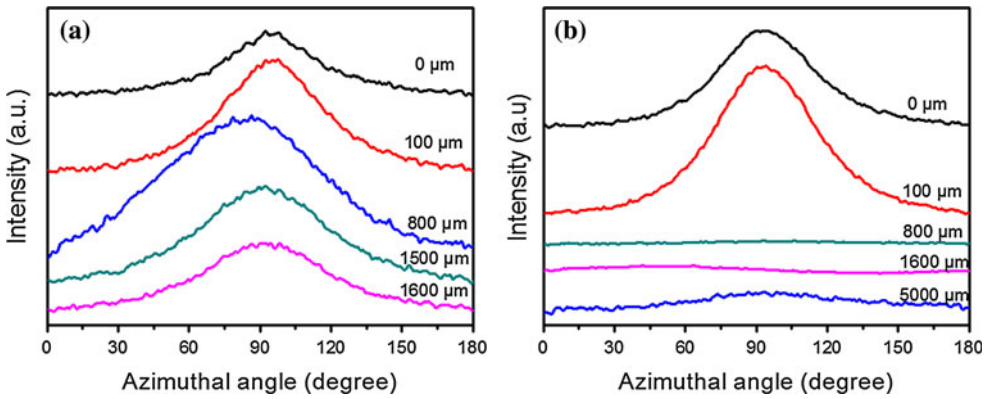

Fig. 5 Traces showing the variation in intensity of the (040) reflection as a function of the azimuthal angle: (**a**) WAIM part and (**b**) CIM part

rate brought by injected water. Nevertheless, for the CIM part, it tends to be 0 at the 800, 1600, and 5000 μm, implying that molecular chains align randomly. This can also be confirmed by the fact that prefect and large spherulites are formed in these regions (see Fig. 3).

It is well known that injection molding process is essentially a flow-induced non-isothermal crystallization process for semi-crystalline polymers. Furthermore, the shear rate, shear stress, and cooling rate are known as the principal factors influencing the orientation of crystals [10–20]. In addition, it is well established that the orientation of polymer molecules is a result of the competition between shear-induced orientation, chain stretching and subsequent relaxation [12–20]. That is, a higher shear rate and/or larger stress lead to a higher level of orientation for molecular chains, while a higher cooling rate slows down the relaxation or even freezes the orientation by the kick-in of crystallization [14–16]. During melt filling, when the iPP melt is injected into mold cavity, an immobile frozen layer is instantaneously formed by cold mold wall, leading

Table 1 The orientation parameters for WAIM and CIM parts

Distance from the skin surface (μm)	WAIM part	CIM part
0	0.549	0.516
100	0.513	0.494
800	0.113	0.048
1500	0.333	
1600	0.365	0.069
5000		0.013

to larger shear stress. The combination of the strong shear stress and low melt temperature generates the oriented structures in skin zone. Owing to the temperature gradient and shear stress attenuation, a delay of crystallization is expected in the zones away from skin, which gives the different time windows for molecules to relax [16]. This can explain the gradual decrease of orientation parameters from skin to core for the CIM part (see Table 1). The detailed description and the mechanism of this phenomenon for CIM parts have been reported previously [14–17].

Therefore, to understand the oriented structures formation mechanism during the WAIM process, the flow behaviors in the separate filling stages (i.e., melt filling process and water penetration process) should be clarified. As mentioned above, both CIM and WAIM processes share a same stage: melt filling. While, the melt is compelled to flow again, accompanying with water injection in the WAIM process. At the end of water penetration, most of the polymer melt in the core of the mold cavity is hollowed out by the injected water and the residual wall (ca. 1.6 mm) is formed. In addition, water penetration can bring about shear flow in the water penetration front (see Supplementary material) and then induce the oriented structure. Furthermore, due to the thinner residual wall of the WAIM part and the high cooling capacity of the water, a pronounced heat exchange occurs (see Supplementary material). Obviously, the oriented structure induced by shear stress could be cooled down rapidly and preserved subsequently. For these reasons, it is evident that the enhanced orientation parameter of the WAIM part should be ascribed to water penetration and the subsequent cooling.

As shown in Fig. 6, the intensity of the (110) reflections are presented as a function of azimuthal angle. At 0 and 100 μm positions of both the parts, the (110) intensity curve shows maxima in the equator (azimuthal angle, $\varphi = 0°$) and in the meridian ($\varphi = 90°$). In contrast, the (040) intensity curves (see Fig. 5) exhibit a maximum in the meridian ($\varphi = 90°$) and a minimum in the equator ($\varphi = 0°$). Similar azimuthal variations were also found by Nogales et al. [21], which can be explained in terms of the parent–daughter model (or the branched shish-kebab structure) [22, 23]. As well known, the parent–daughter model is a mixed bimodal orientation and corresponding with the bimodal (110) reflections, i.e., parent lamellae (or c-axis-oriented component) is preferentially oriented to the flow direction, whereas the daughter lamellae (or a*-axis-oriented component) is preferentially perpendicular to the flow direction [22–27].

A relative comparison between parent lamellae and daughter lamellae orientations can be made from calculation of the fraction of daughter lamellae ($[A^*]$). $[A^*]$ can be evaluated from the azimuthal scan curve of the (110) reflection according to Fujiyama's method [23]:

$$[A^*] = \frac{A^*}{C + A^*} \tag{3}$$

where A^* is taken as the area around an azimuthal angle of 0° and C represents the area around 90°, after subtraction of the baseline area (see Fig. 6a). The fraction of daughter lamellae of the CIM part at 0 and 100 μm is 0.585 and 0.749, respectively, and 0.561 and 0.686 for the WAIM one. It is clear that the fraction of daughter lamellae for WAIM part had the low values near the skin zone, suggesting that daughter lamellae are suppressed by the rapid cooling rate brought by injected water. Furthermore, for CIM part, the fraction of daughter lamellae increases with increasing the distance from the skin surface because of the

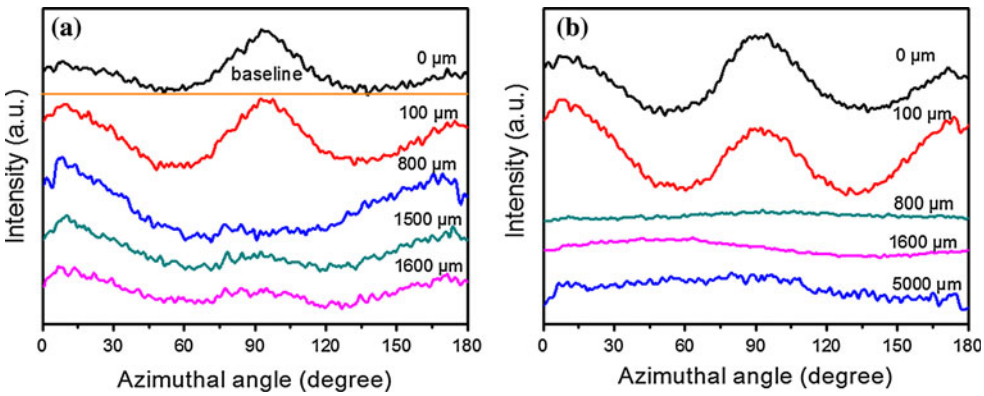

Fig. 6 Traces showing the variation in intensity of the (110) reflections as a function of the azimuthal angle: (**a**) WAIM part and (**b**) CIM part

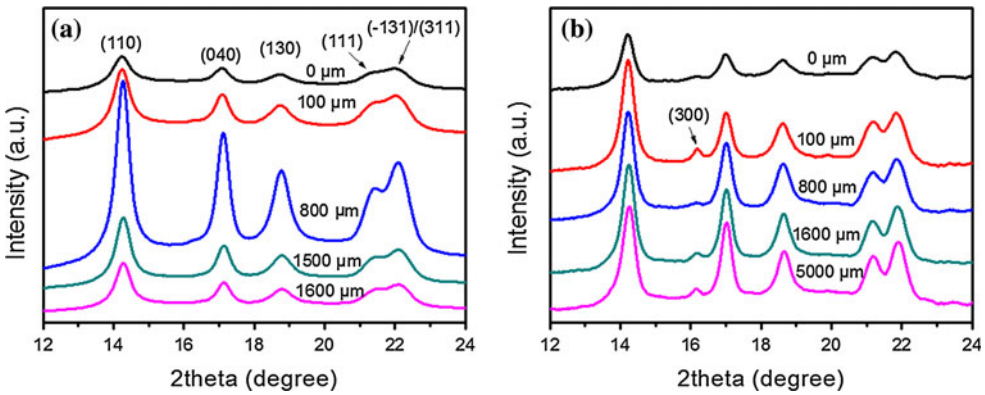

Fig. 7 1D-WAXD curves of (**a**) WAIM part and (**b**) CIM part obtained from circularly integrated intensities of 2D-WAXD patterns in Fig. 4

temperature gradient from skin to core zone, which is in a good agreement with that in the literatures [25–27].

Crystallization

To get more insights into crystallization, the peak-fit procedure was employed to deconvolute the peaks in the 1D-WAXD profile. Figure 7 shows the 1D-WAXD curves obtained from circularly integrated intensities of 2D-WAXD patterns in Fig. 4. Herein, the X-ray curves were resolved into crystalline and amorphous peaks. The overall crystallinity (X_c) was calculated by

$$X_c = \frac{\sum A_{\text{cryst}}}{\sum A_{\text{cryst}} + \sum A_{\text{amorp}}} \tag{4}$$

where A_{cryst} and A_{amorp} are the fitted areas of the crystalline and amorphous phases. The estimated crystallinity data is shown in Table 2. The crystallinity of the WAIM is consistently lower than that of the CIM part at the same distance from the skin surface. Furthermore, the crystallinity for the WAIM part first increases and then decreases with the elevating distance from the skin surface, while that of CIM part tends to increase monotonously. Higher cooling rate appears in the skin zone of both the part as well as the water channel zone of the WAIM part, resulting in a lower degree of overall crystallinity.

Interestingly, from Fig. 7, it is noticed that in all the positions of the CIM part there is a very tiny (300) reflection for β-form. However, it is invisible in all the positions for the WAIM part. This finding confirmed the POM observation. According to the method proposed by Turner-Jones [35], the relative amount of the β-form crystal (K_β) was calculated and shown in Table 2. It is widely accepted that shearing of iPP melt causes the formation of α-row nuclei and a subsequent growth of the β-phase on the formed α-row nuclei [36]. For the WAIM part, the fast solidifying rate brought by injected water leaves short time for the growth of the β-phase on the formed α-row nuclei, leading to the absence of β-form crystals. However, it is confused that a certain amount of

Table 2 The crystallinity as well as K_β for WAIM and CIM parts

Distance from the skin surface (μm)	Crystallinity (%)		K_β (%)	
	WAIM part	CIM part	WAIM part	CIM part
0	49.5	52.6	0	0.8
100	50.9	55.4	0	2.2
800	59.3	59.4	0	0.4
1500	55.1		0	
1600	54.3	60.0	0	0.9
5000		60.9		1.1

β-form crystals emerge in the core region of the CIM part. As well established, the injection molded iPP contains a larger amount of β-form crystals in the skin zone, while an extremely smaller quantity of β-form crystals in the core zone [28–34]. Seemingly, our study contradicts these previous studies. Further study on the underlying reason for this is undergoing in our group.

The crystallite size of each plane can be calculated from diffraction peaks of WAXD using the Scherrer equation [37]:

$$L = \frac{K\lambda}{\beta_{hkl}\cos\theta_{hkl}} \tag{5}$$

where L_{hkl} is the crystallite diameter (hkl), λ is the wave length of the X-ray, K is crystallite shape factor, θ_{hkl} is the Bragg angle and β_{hkl} is the width of the diffraction peak. β_{hkl} can be calculated by the equation: $\beta_{hkl} = \left(b^2 - b_0^2\right)^{1/2}$, where b is the samples half-peak width, and b_0 is the instrumental resolution.

Table 3 shows the distribution of the crystallite size L, and the d-spacing of crystal planes along the thickness of both the parts. In general, for WAIM part, the crystallite size L through the thickness from skin surface to water channel surface tends to elevate first and then decreases with the increase of the distance till the water channel surface. The crystallite size L for the CIM part continuously increases, but the value is slightly larger than that of

Table 3 *d*-spacing and crystallite size *L* for the WAIM and CIM parts at different positions

Part	Distance from the skin surface (μm)	*d*-spacing (Å)			*L* (nm)		
		(110)	(040)	(130)	(110)	(040)	(130)
WAIM	0	6.256	5.214	4.766	12.1	20.9	14.2
	100	6.256	5.221	4.759	13.6	21.4	14.5
	800	6.250	5.210	4.755	17.4	22.5	15.8
	1500	6.246	5.210	4.755	15.3	21.3	14.5
	1600	6.246	5.210	4.755	14.8	21.2	14.2
CIM	0	6.246	5.210	4.759	13.7	20.4	14.3
	100	6.246	5.210	4.759	15.6	22.4	15.2
	800	6.243	5.210	4.755	17.9	24.1	16.6
	1600	6.243	5.210	4.755	19.0	25.4	17.3
	5000	6.243	5.210	4.755	19.5	26.2	18.0

the WAIM part in the corresponding position. It is noted that the decrease in crystallinity is consistent with the thinning of crystalline lamellae [38]. Moreover, *d*-spacing of crystal planes decreases from the skin surface for the both the parts. However, there is a difference in the values of *d*-spacing for the WAIM and CIM parts, that is, the former is slightly larger than the latter at the same distance from the skin surface. The *d*-spacing of crystal planes of iPP increases and the crystallite size *L* decreases in the skin and water channel zone, indicating that the crystal particles pack looser. This finding is in consistent with the Reference [39]. They are mainly attributed to the rapid cooling rate in the skin and water channel zone.

Conclusion

Morphologies of iPP parts molded by WAIM and CIM were comparatively investigated by means of POM and 2D-WAXD. POM observations showed that the WAIM part exhibits a "skin–core–water channel" structure, which is different from the typical "skin–core" structure for the CIM part. The 2D-WAXD pattern of WAIM part showed arclike reflections in all positions indicating a pronounced molecular orientation of iPP. However, pronounced orientation is only found at 0 and 100 μm for the CIM part. Furthermore, a parent–daughter model (or branched shish-kebab structure) observed from (110) reflection appears at 0 and 100 μm for both the parts. In addition, from the 1D-WAXD curves, it is noticed that there is a very tiny (300) reflection for β-form in the CIM part, while it is invisible in all the positions of the WAIM part. Meanwhile, water penetration and rapid cooling rate brought by water plays an important role in the decrease of the fraction of daughter lamellae, crystallinity, and crystalline size *L*. The rapid cooling rate and shear brought by the water penetration are the two principal factors in the oriented structures formation. In summary, the results showed that the water penetration has a dramatic effect on the morphological development through the thickness of the WAIM part.

Acknowledgements The authors thank National Natural Science Foundation of China for financial support (Grant No. 50803060, 10872185, and 10872186) and the authors also thank Prof. Guoqiang Pan and Liangbin Li from National Synchrotron Radiation Laboratory (NSRL) in University of Science and Technology of China for their help in synchrotron 2D-WAXD experiment.

References

1. Knights M (2002) Plast Technol 48:42
2. Liu SJ, Su PC (2009) Polym Test 28:66
3. Liu SJ, Lin MJ, Wu YC (2007) Compos Sci Technol 67:1415
4. Huang HX, Deng ZW (2008) J Appl Polym Sci 108:228
5. Lin KY, Liu SJ (2010) Macromol Mater Eng 295:342
6. Liu SJ, Lin WR, Lin KY (2010) Morphological development in water assisted injection molded polyethylene/polyamide-6 blends. Polym Adv Technol. doi:10.1002/pat.1721
7. Huang HX, Zhou RH (2010) Polym Test 29:235
8. Liu SJ, Wu YC (2007) Polym Test 26:232
9. Liu XH, Zheng GQ, Jia ZH, Li SW, Liu CG, Zhang Y, Shao CG, Dai K, Liu BC, Zhang QX, Wang SJ, Liu CT, Chen JB, Peng XF, Shen CY (2011) The hierarchical structure of water-assisted injection molded HDPE: SAXS study. J Appl Polym Sci. (in press)
10. Wang Y, Gao Y, Shi J (2008) J Appl Polym Sci 107:309
11. Wang Y, Na B, Fu Q, Men YF (2004) Polymer 45:207
12. Zhu PW, Edward G (2004) Macromolecules 37:2658
13. Zhu PW, Tung J, Edward G (2005) Polymer 46:10960
14. Zheng GQ, Yang W, Yin B, Yang MB, Liu CT, Shen CY (2006) J Appl Polym Sci 2006(102):3069
15. Zheng GQ, Huang L, Yang W, Yang B, Yang MB, Li Q, Shen CY (2007) Polymer 48:5486
16. Zhong GJ, Li LB, Mendes E, Byeloy D, Fu Q, Li ZM (2006) Macromolecules 39:6771
17. Zhong GJ, Li ZM, Li LB, Mendes E (2007) Polymer 48:1729
18. Picken SJ, Aerts J, Visser R, Northolt MG (1990) Macromolecules 23:3849
19. Kumaraswamy G, Verma RK, Kornfield JA, Yeh F, Hsiao BS (2004) Macromolecules 37:9005
20. Somani RH, Hsiao BS, Nogales A, Fruitwala H, Srinivas S, Tsou AH (2001) Macromolecules 34:5902
21. Nogales A, Mitchell GR, Vaughan AS (2003) Macromolecules 36:4898
22. Fujiyama M, Wakino T, Kawasaki Y (1988) J Appl Polym Sci 35:29
23. Lotz B, Wittmann JC (1986) J Polym Sci Part B 24:1541
24. Zhu PW, Tung J, Edward G, Nichols L (2008) J Appl Phys 103:124906
25. Zhu PW, Phillips A, Tung J, Edward G (2005) J Appl Phys 97:104908
26. Zhu PW, Edward G (2008) J Mater Sci 43:6459
27. Schrauwen BAG, Breemen LCAv, Spoelstra AB, Govaert LE, Peters GWM, Meijer HEH (2004) Macromolecules 37:8618
28. Obadal M, Čermák R, Raab M, Vincent V, Commereuc S, Fraïsse F (2006) Polym Degradation Stab 91:459

29. Li YB, Shen KZ (2008) J Macromol Sci B 47:1000
30. Bai HW, Wang Y, Zhang ZJ, Han L, Li YL, Liu L, Zhou ZW, Men YF (2009) Macromolecules 42:6647
31. Bai HW, Wang Y, Song B, Li YL, Liu L (2008) Polym Eng Sci 48:1532
32. Chen YH, Zhong GJ, Wang Y, Li ZM, Li LB (2009) Macromolecules 42:4343
33. Kalay G, Bevis MJ (1997) J Polym Sci B 35:241
34. Fujiyama M (1995) Int Polym Process 10:172
35. Turner-Jones A, Aizelwood JM, Beckett DR (1964) Macromol Chem 75:134
36. Varga J, Karger-Kocsis J (1995) Polymer 36:4877
37. Alexander LE (1976) X-ray diffraction methods in polymer science. Wiley, New York
38. Zhu PW, Tung J, Phillips A, Edward G (2006) Macromolecules 39:1821
39. Kang J, Chen JY, Cao Y, Li HL (2010) Polymer 51:249